

Electronic Supplementary Information for

Heteroleptic Cationic Iridium(III) Complexes Bearing Phenanthroline Derivatives with Extended π -Conjugation as Potential Broadband Reverse Saturable Absorbers

Li Wang,^a Peng Cui,^{a,b} Levi Lystrom,^a Jiapeng Lu,^a Svetlana Kilina^a and Wenfang Sun^{a,}*

^a Department of Chemistry and Biochemistry, ^b Materials and Nanotechnology Program, North Dakota State University, Fargo, North Dakota 58108-6050, United States

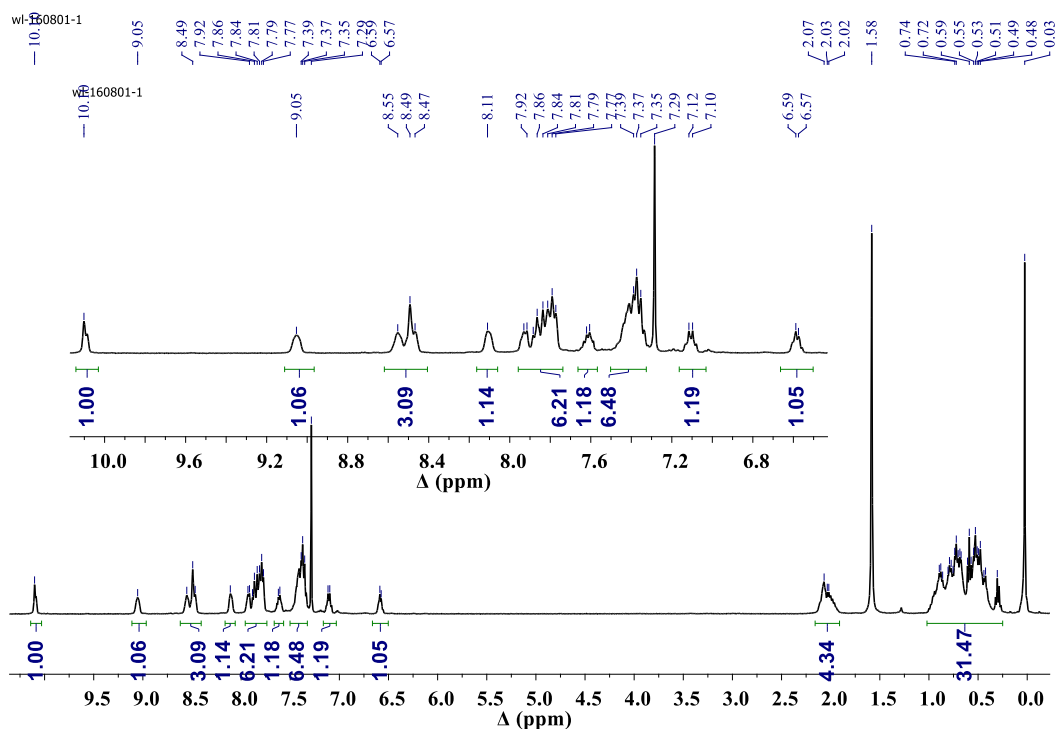


Fig. S1 ^1H NMR spectrum of complex **2** in CDCl_3 .

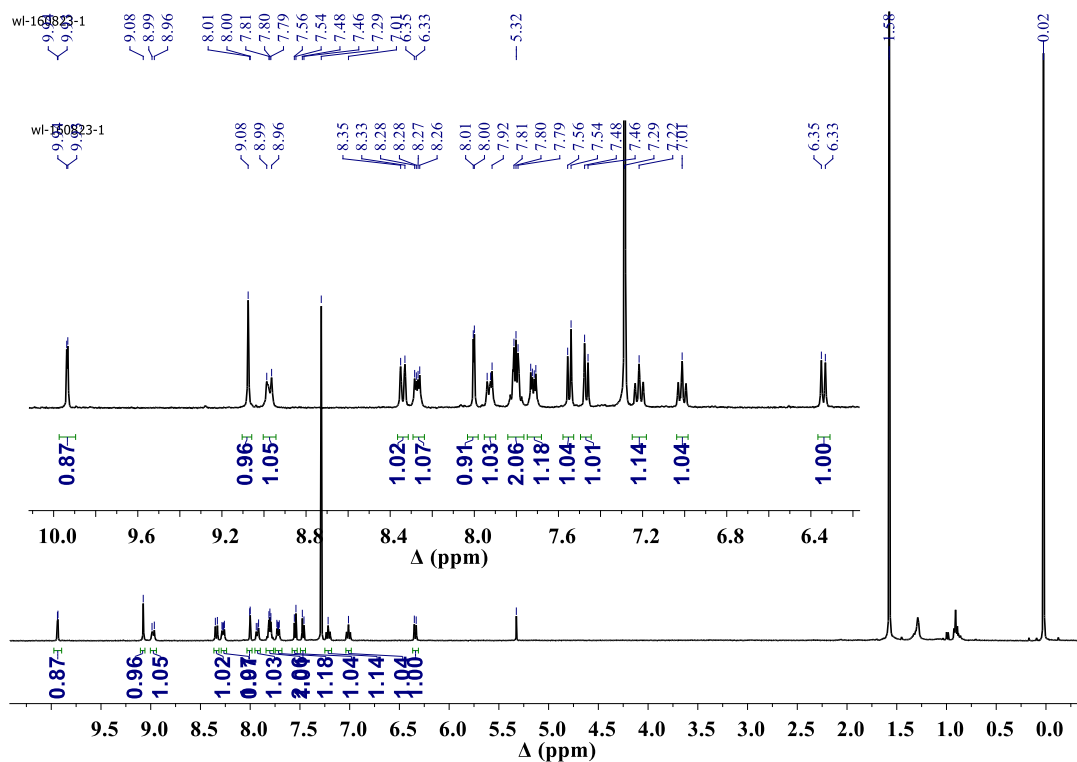


Fig. S2 ^1H NMR spectrum of complex $\text{Ir}(\text{piq})_2(\text{dppn-2Br})$ in CDCl_3 .

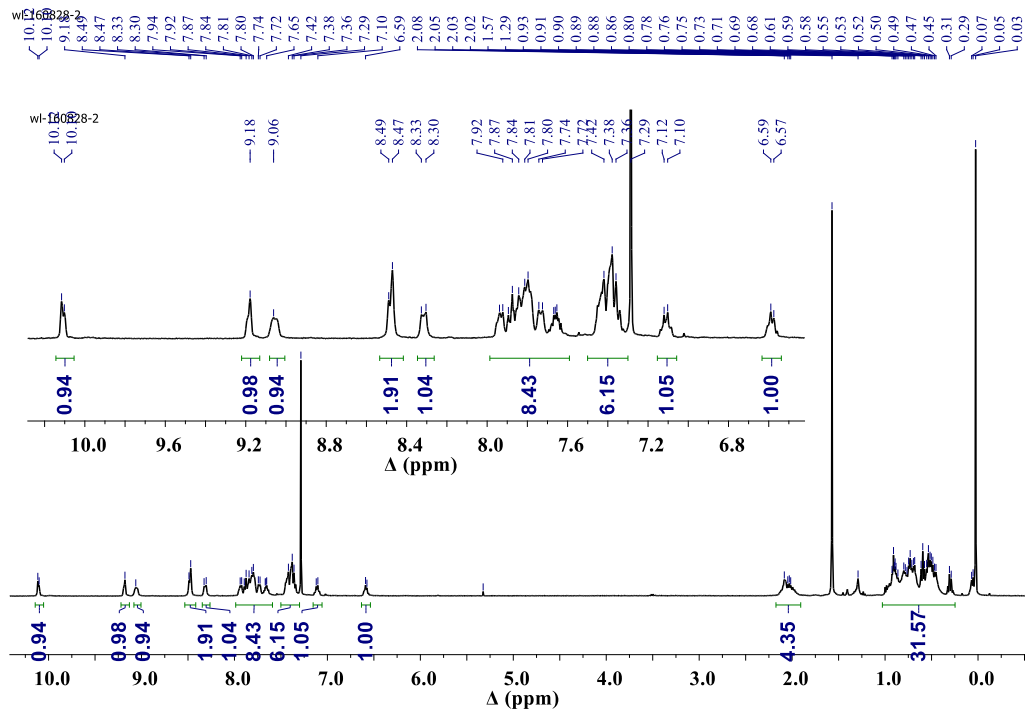


Fig. S3 ^1H NMR spectrum of complex **3** in CDCl_3 .

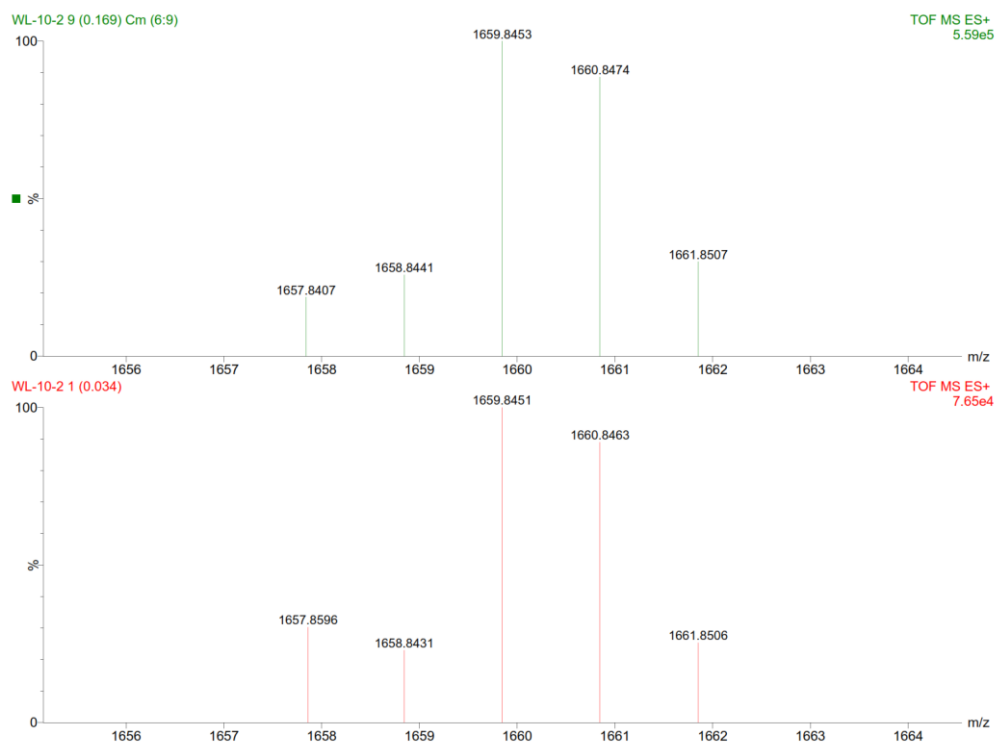


Fig. S4 HRMS spectra of complex **2**. Top: theoretical spectrum calculated for $\text{C}_{106}\text{H}_{110}\text{IrN}_6$ (M-PF_6); Bottom: experimental spectrum.

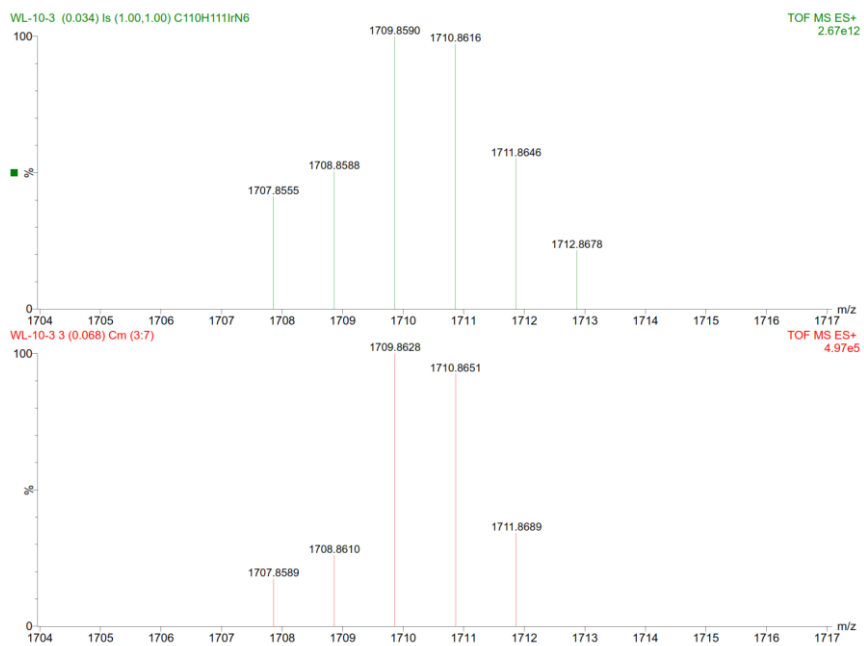


Fig. S5 HRMS spectra of complex **3**. Top: theoretical spectrum calculated for C₁₁₀H₁₁₂IrN₆ (M-PF₆); Bottom: experimental spectrum.

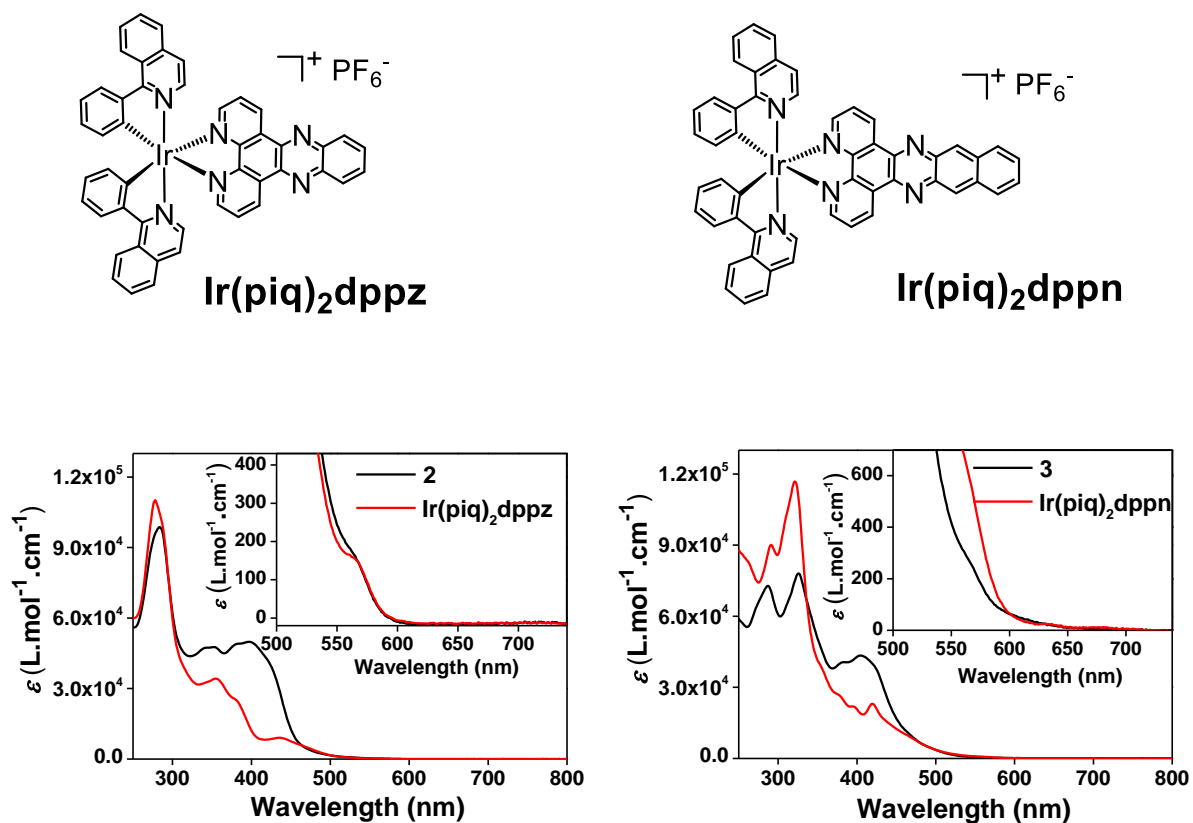


Fig. S6 Comparison of the UV-vis absorption spectra of complexes **2** and **3** to those of their corresponding complexes without the fluorenyl substituents **Ir(piq)₂dppz** and **Ir(piq)₂dppn** in acetonitrile solutions.

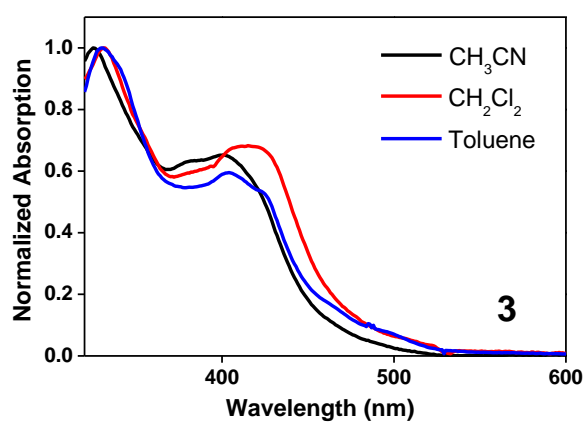
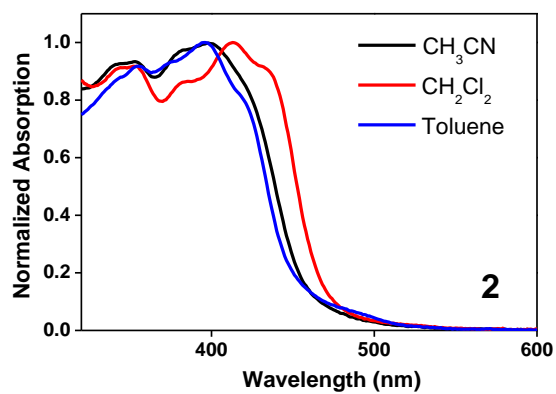
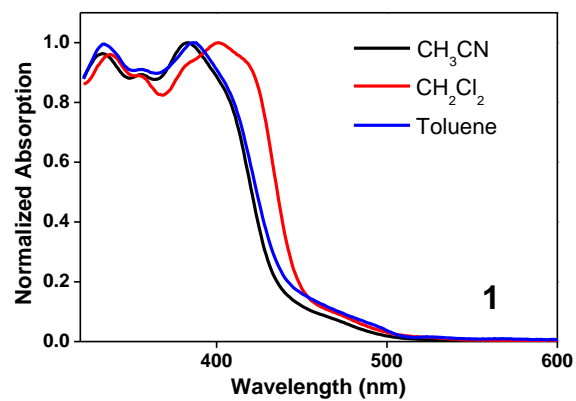


Fig. S7 Normalized UV-vis absorption spectra of complexes **1-3** in different solvents.

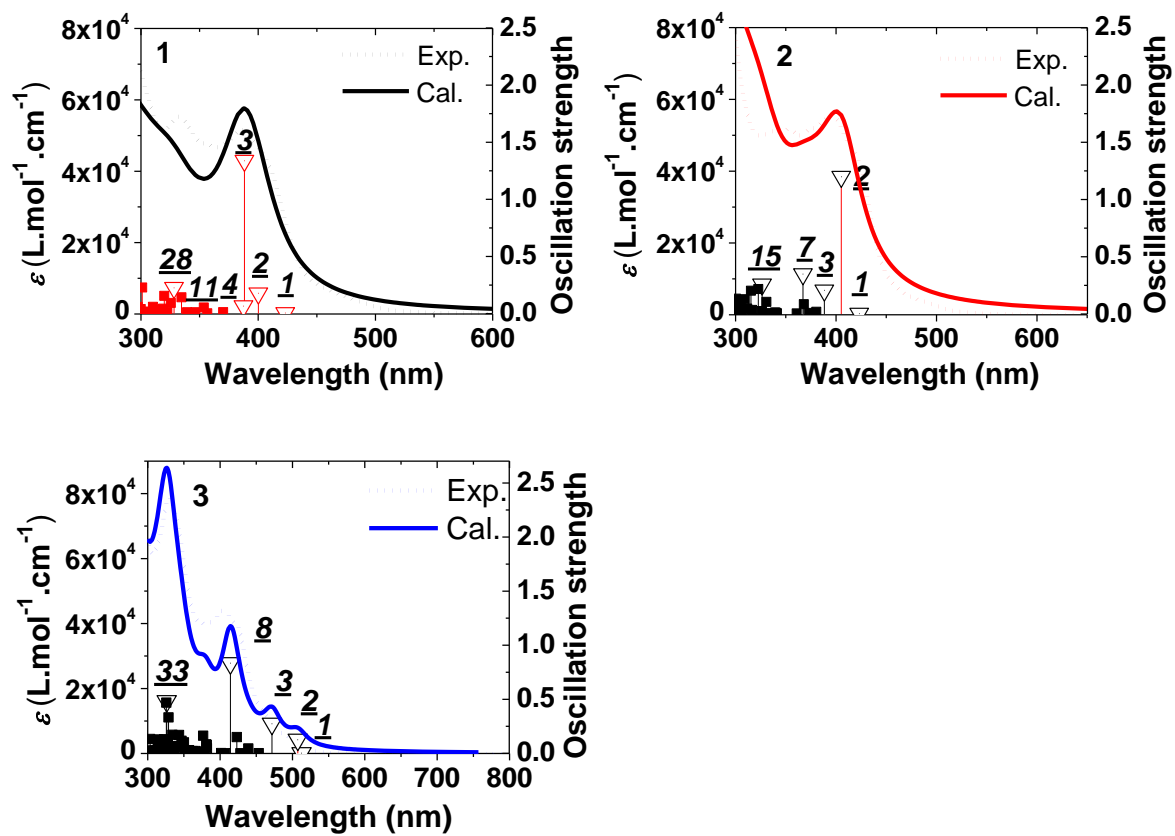
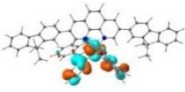
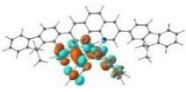
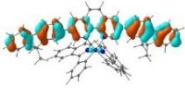
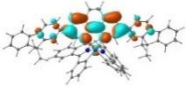
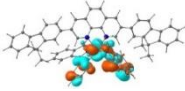
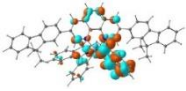
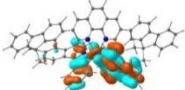
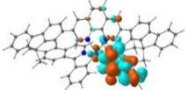
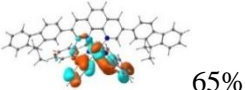
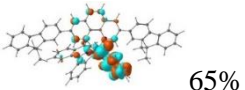
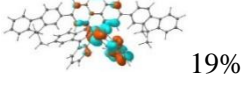
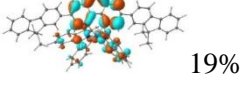
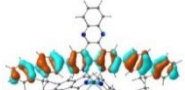
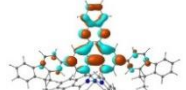
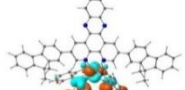
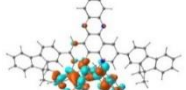
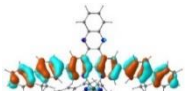
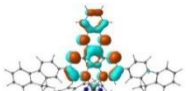
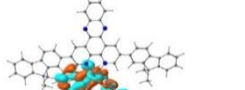
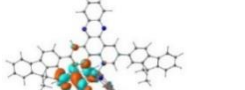
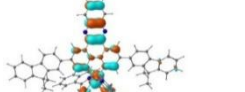
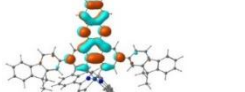


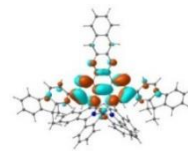
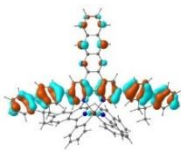
Fig. S8 Comparison of the experimental and calculated UV-vis absorption spectra of complexes **1-3** in toluene.

Table S1 Natural transition orbitals (NTOs) representing main absorption bands for complexes **1-3** in toluene.

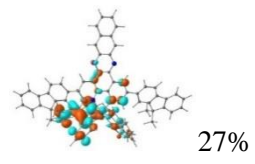
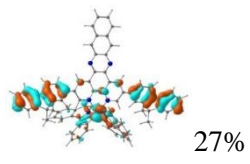
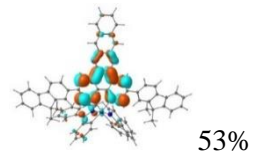
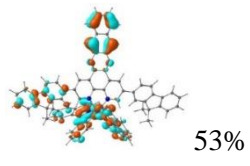
| | S_n | Holes | Electrons |
|----------|----------------------------------|---|---|
| 1 | S_2 401 nm $f = 0.18$ |  |  |
| | S_3 389 nm $f = 1.34$ |  |  |
| | S_4 388 nm $f = 0.07$ |  |  |
| | S_{11} 329 nm $f = 0.23$ |  |  |
| | S_{28} 290 nm $f = 0.06$ |  65% |  65% |
| | |  19% |  19% |
| 2 | S_2 406 nm $f = 1.20$ |  |  |
| | S_3 389 nm $f = 0.21$ |  |  |
| | S_7 368 nm $f = 0.35$ |  |  |
| | S_{15} 327 nm $f = 0.26$ |  67% |  67% |
| | |  17% |  17% |

3

S_8
415 nm
 $f = 0.83$



S_{33}
327 nm
 $f = 0.48$



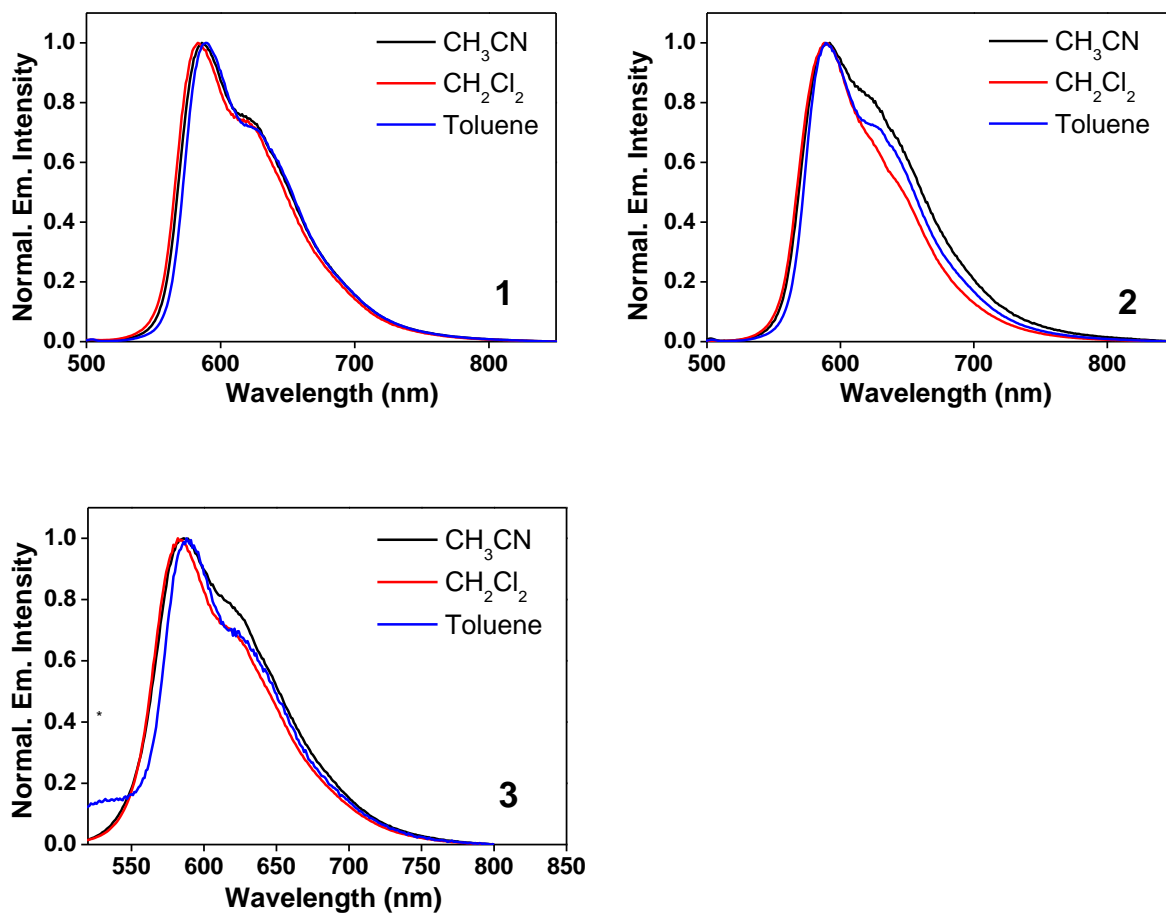
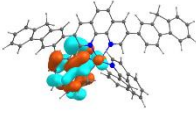
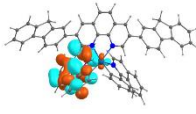
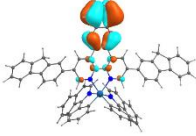
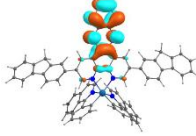
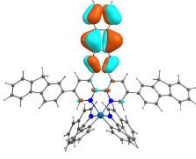
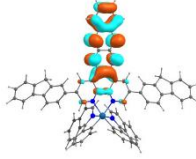
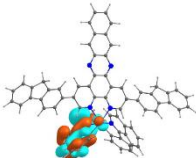
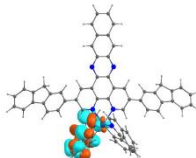


Fig. S9 Normalized emission spectra of complexes **1-3** in different solvents at room temperature. $\lambda_{\text{ex}} = 436$ nm.

Table S2 Emission band maxima (λ_{em}), lifetimes (τ_{em}) and quantum yields (Φ_{em}) for complexes **1-3** in different solvents at room temperature.

| | λ_{em}/nm ($\tau_{em}/\mu s$); Φ_{em} | | |
|----------|--|---------------------------------|-------------------|
| | CH ₃ CN | CH ₂ Cl ₂ | Toluene |
| 1 | 586 (3.30); 0.35 | 583 (3.80); 0.40 | 590 (3.10); 0.46 |
| 2 | 590 (1.05); 0.13 | 590 (4.42); 0.57 | 590 (2.93); 0.40 |
| 3 | 587 (2.37); 0.035 | 588 (2.84); 0.077 | 590 (2.00); 0.003 |

Table S3 Natural transition orbitals (NTOs) of the low(est)-energy triplet transitions of **1-3** in acetonitrile.

| | T_n | Hole | Electron |
|----------|-----------------|---|---|
| 1 | T_1 910 nm |  |  |
| 2 | T_1 905 nm |  |  |
| 3 | T_1 935 nm |  |  |
| | T_2 909 nm |  |  |

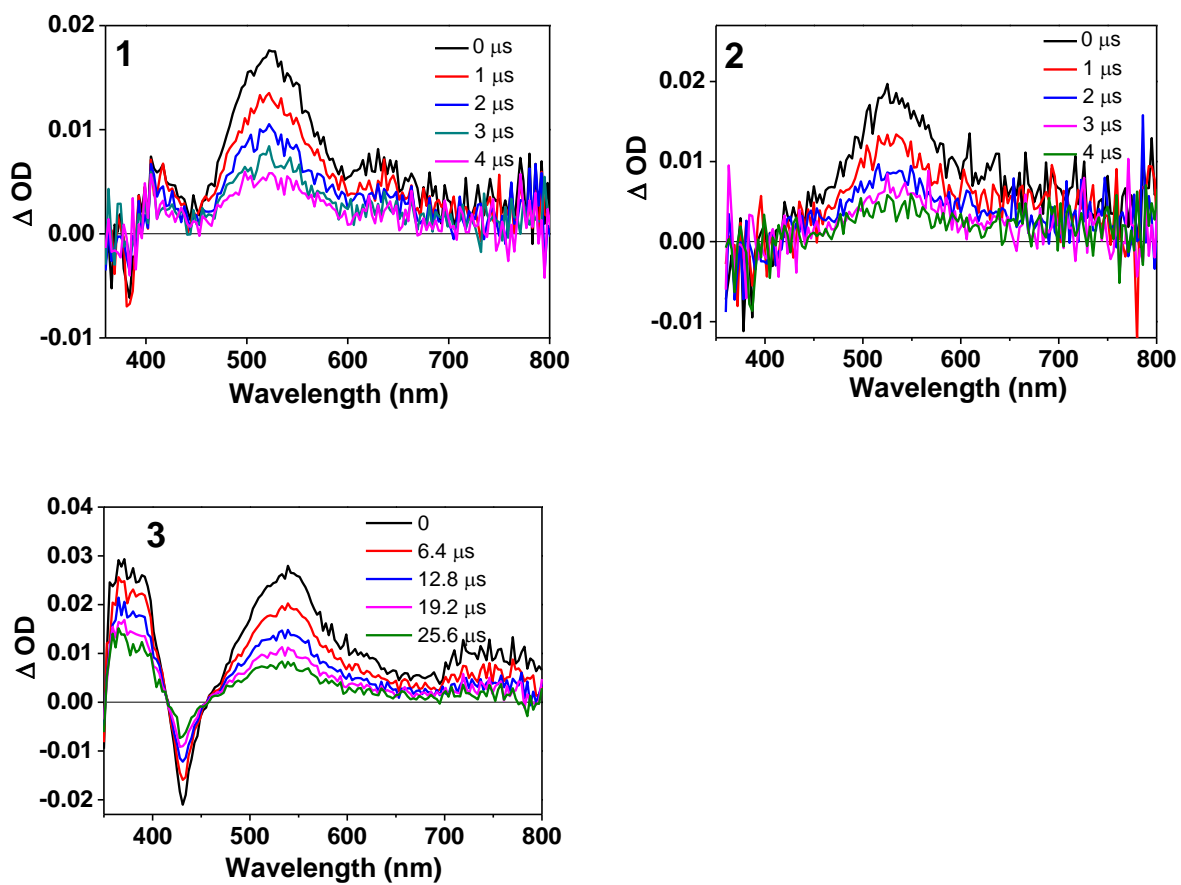


Fig. S10 Time-resolved ns transient absorption spectra of complexes **1-3** in deoxygenated toluene. $\lambda_{\text{ex}} = 355 \text{ nm}$, $A_{355 \text{ nm}} = 0.4$ in a 1-cm cuvette.

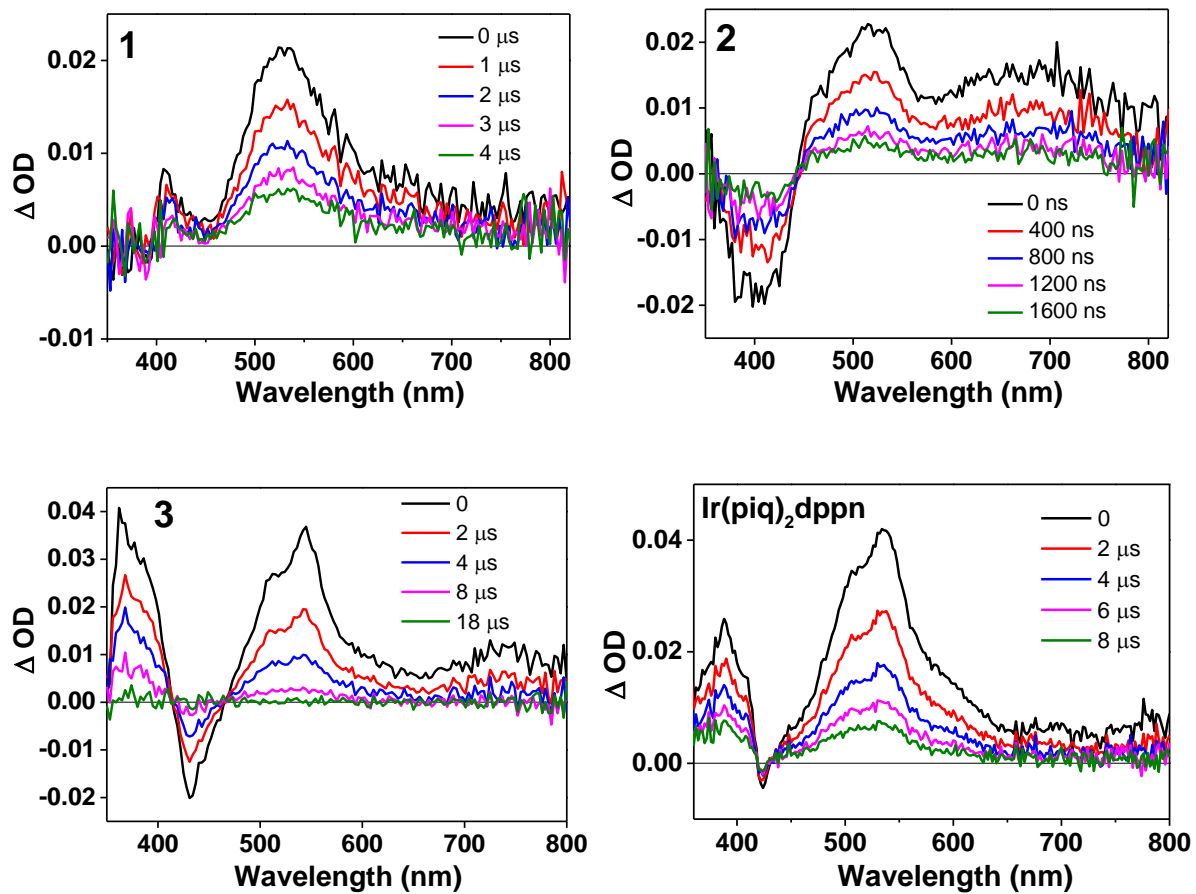


Fig. S11 Time-resolved ns transient absorption spectra of complexes **1-3** and complexes **Ir(piq)₂dppn** in deoxygenated acetonitrile. $\lambda_{\text{ex}} = 355 \text{ nm}$, $A_{355 \text{ nm}} = 0.4$ in a 1-cm cuvette.

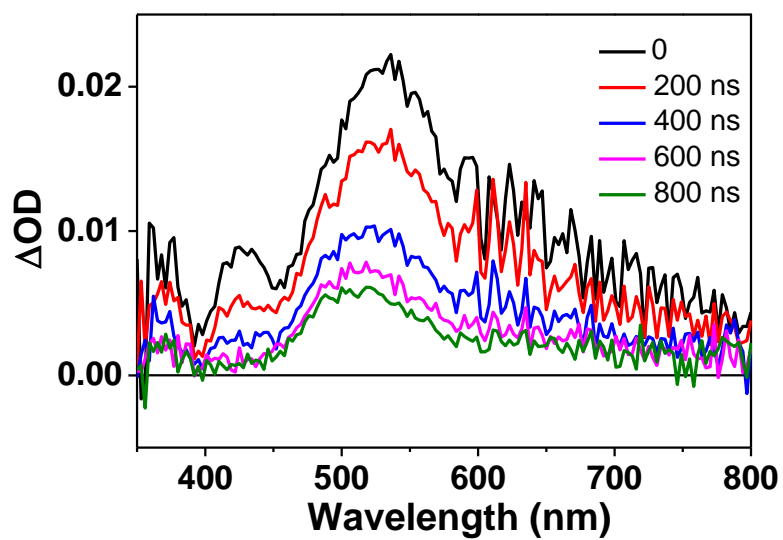


Fig. S12 Time-resolved ns transient absorption spectra of [Ir(piq)₂Cl]₂ in deoxygenated acetonitrile. $\lambda_{\text{ex}} = 355 \text{ nm}$, $A_{355 \text{ nm}} = 0.4$ in a 1-cm cuvette.

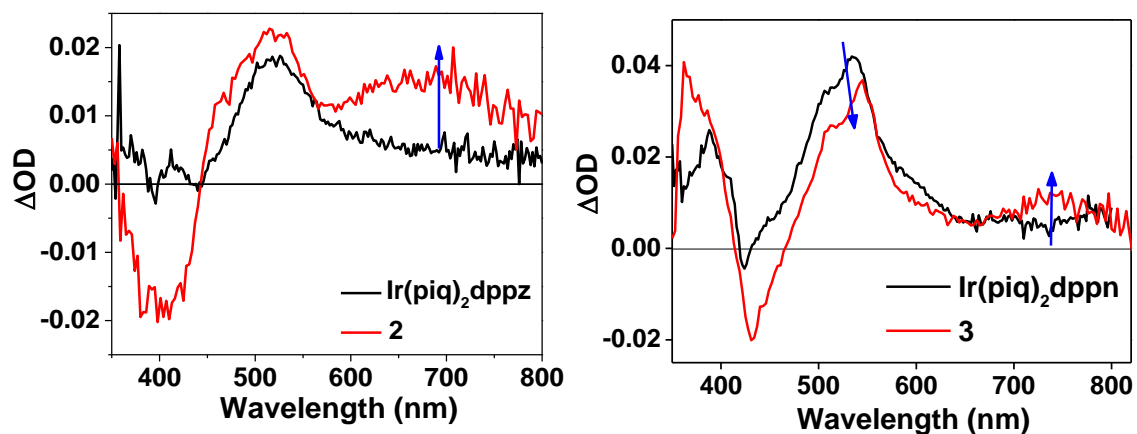


Fig. S13 Comparison of ns transient absorption spectra at zero-time delay for complexes **2** and **3** with $\text{Ir}(\text{piq})_2\text{dppz}$ and $\text{Ir}(\text{piq})_2\text{dppn}$, respectively, in deoxygenated acetonitrile. $\lambda_{\text{ex}} = 355 \text{ nm}$, $A_{355 \text{ nm}} = 0.4$ in a 1-cm cuvette.

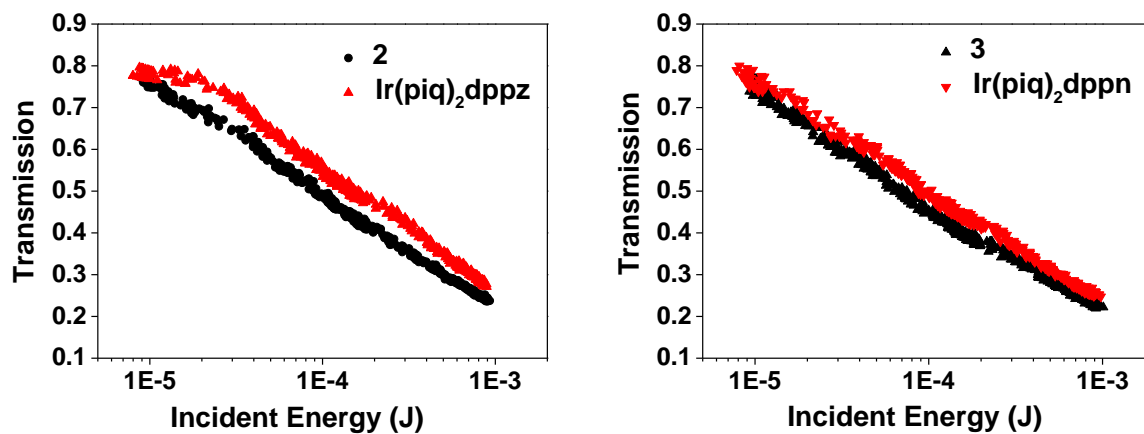


Fig. S14 Comparison of RSA performance of complex **2** with **Ir(piq)₂dppz** and complex **3** with **Ir(piq)₂dppn** in acetonitrile for 4.1-ns laser pulses at 532 nm in a 2-mm cuvette. The linear transmission was adjusted to 80% at 532 nm for each sample in a 2-mm cuvette.